Effect of support structure of Pt/silicaite-1 catalyst on non-thermal plasma (NTP) assisted chlorobenzene degradation and PCDD/Fs formation

Yibing Mu [a], Yilai Jiao [b], Xinrui Wang [c], Paul T. Williams [a],*

[a] School of Chemical and Process Engineering, University of Leeds, Leeds, LS2 9JT, UK
[b] Shenyang National Laboratory for Materials Science, Institute of Metal Research, Chinese Academy of Science, 110016, China
[c] Department of Chemical Engineering, The University of Manchester, Manchester, M13 9PL, UK

HIGHLIGHTS

- Cl–VOCs are decomposed by a non-thermal plasma catalysis process.
- Nano-sized Pt on hierarchical silicaite support decomposes Cl–VOCs.
- Catalyst pore structure significantly impacts Cl-VOC decomposition.
- Pore structure also affects by-product formation (PCCD/F).

GRAPHICAL ABSTRACT
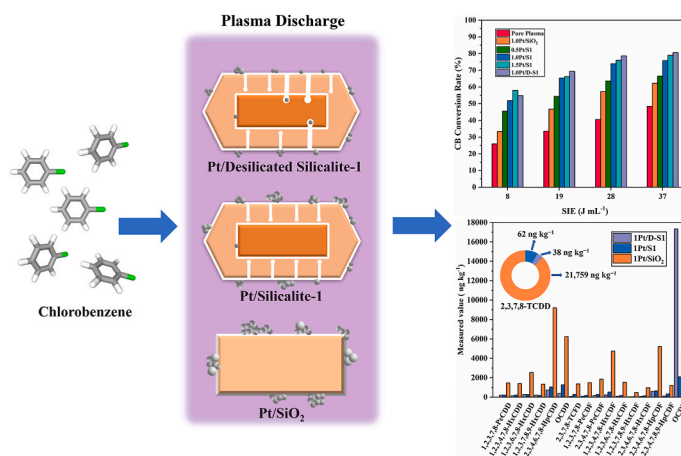
ARTICLE INFO

Handling editor: E. Brillas

ABSTRACT

Development of efficient catalysts for non-thermal plasma (NTP) assisted catalysis to mitigate the formation of harmful by-products is a significant challenge in the degradation of chlorinated volatile organic compounds (Cl–VOCs). In this study, catalytically active Pt nanoparticles supported on non-porous SiO2 and silicalite-1 zeolites (S1) with different pore structure were comparatively investigated for catalytic chlorobenzene degradation under NTP condition. It was shown that the pore structure could significantly impact the metal size and metal dispersion rate. Pt supported on modified S1 hierarchical meso-micro-porous silicalite-1 (Pt/D-S1) exhibited the smallest particle size (~6.19 nm) and the highest dispersion rate (~1.87). Additionally, Pt/D-S1 demonstrated superior catalytic performance compared to the other catalysts, achieving the highest chlorobenzene conversion and COx selectivity at about 80% and 75%, respectively. Furthermore, the pore structure also affected the formation of by-products according to the findings from GC-MS analysis. Pt/SiO2 generated a total of 18 different species of organic compounds, whereas only 12 species of organic by-products were identified in the Pt/D-S1 system (e.g. polychlorinated compounds like 3,4 dichlorophenol were exclusively identified

* Corresponding author.
  E-mail address: p.t.williams@leeds.ac.uk (P.T. Williams).

in Pt/SiO$_2$). Moreover, dioxin-like polychlorinated biphenyl and other chlorinated organic compounds, which have potential to form highly toxic dioxins, were detected in the catalysts. HRGC-HRMS confirmed and quantified the 17 different dioxin/furans formed on Pt/SiO$_2$ (25,100 ng TEQ kg^{-1}), Pt/S1 (515 ng TEQ kg^{-1}) and Pt/D-S1 (367 ng TEQ kg^{-1}). The correlation between synthesis-structure-performance in this study provides insights into the design of catalysts for deep oxidation of Cl–VOCs in NTP system.

1. Introduction

Chlorinated volatile organic compounds (Cl–VOCs), a significant subset of volatile organic compounds (VOCs), are recognised as major contributors to global air and water pollution due to their low biodegradability, high stability, and toxicity (EPA, 2014; Mu and Williams, 2022). Moreover, many Cl–VOCs, such as trichloroethylene, tetrachloroethylene, and dichloromethane, have been identified as carcinogenic to human beings by the International Agency for Research on Cancer (Fletcher et al., 2002). The emissions of Cl–VOCs lead to the formation of ozone, photochemical smog, and secondary organic aerosol (Choi et al., 2020; Lin et al., 2021b; Whalley et al., 2021). In contrast to other VOCs, the chlorine substitution in Cl–VOCs results in their degradation and becomes more challenging and complicated, as well as generating highly toxic secondary pollutants, such as polychlorinated compounds, polychlorinated dibenzo-p-dioxins (dioxins (PCDDs)) and polychlorinated dibenzofurans (furans (PCDFs)). Hence, there is an urgent need for the development of technologies aimed at efficiently degrading Cl–VOCs and mitigating the production of toxic by-products.

Chlorobenzene is extensively used as a solvent in various industrial applications and served as a crucial intermediate in chemical synthesis. It is considered the most hazardous member of Cl–VOCs and has attracted significant research attention due to its role as a key precursor in the formation of highly toxic dioxins (Yeh et al., 2020; Lin et al., 2021a). Therefore, chlorobenzene was selected as the model component for this study to explore methods for achieving deep oxidation of Cl–VOCs and minimising the formation of toxic by-products.

Non-thermal plasma (NTP)-assisted catalysis is recognised as a promising technology in Cl–VOCs degradation due to the unique interplay between plasma and heterogeneous catalysts (Chen et al., 2019, 2020a, 2020b). Numerous efforts have been dedicated to studying the degradation of Cl–VOCs under NTP conditions. For example, the utilisation of MnOx/γ-Al$_2$O$_3$ has been explored for the degradation of chlorobenzene under NTP conditions (Li et al., 2021b). The NTP-assisted catalysis system exhibited remarkable efficiency, eliminating nearly all injected chlorobenzene with a conversion rate of 98%. However, a significant portion of the degraded chlorobenzene was transformed into other organic chemicals, yielding a selectivity of 21% for the desired CO$_2$. Furthermore, investigations into noble metal-based catalysts in NTP-assisted Cl–VOCs degradation have demonstrated enhanced CO$_2$ selectivity. For example, the utilisation of 1 wt% Ag/TiO$_2$ for chlorobenzene degradation resulted in an 88% removal efficiency and a notable 51% COx selectivity (Zhu et al., 2015).

The formation of final products in the degradation of Cl–VOCs becomes considerably more intricate owing to the presence of chlorine in the chemical structure (Lei et al., 2019; Lin et al., 2021b). Various investigations have been undertaken to enhance Cl–VOCs degradation through NTP-assisted catalysis. For example, the humidity level within the system has been identified as a factor influencing both CO$_2$ formation and HCl selectivity (Abedi et al., 2018; Zhou et al., 2021). The NTP-assisted Cl–VOCs degradation is also beneficial from the ·OH radicals generated by the injected water. Similarly, catalysts featuring abundant acidity sites have been demonstrated to improve CO$_2$ and HCl selectivity while mitigating the formation of by-products (Yang et al., 2017b; Weng et al., 2018; Sun et al., 2020; Li et al., 2021b). Despite the number of studies performed, to date, information concerning the control of by-products remains limited. The prevention of dioxins formation in NTP-assisted Cl–VOCs systems is notably lacking, even though

PCDD/Fs have been detected on the surface of catalysts following NTP-assisted catalytic degradation (Altarawneh et al., 2009; Yu et al., 2022).

Porous materials are extensively employed as catalyst supports owing to their commendable porous structure, acidic properties, and hydrothermal stability (García-Martínez et al., 2012; Chen et al., 2021; Wang et al., 2021). In NTP systems, the accessibility of metal active sites plays a crucial role in determining the performance of NTP-assisted catalysis. Consequently, understanding the impact of the porous network on the diffusion of plasma-induced species is essential for the tailored design of NTP catalysts. It is widely accepted that the diffusion of plasma and short-lived reactive species is more challenging in micropores (Xu et al., 2023). The limited accessibility of metal active sites occurs because short-lived reactive species can only penetrate the boundary layer of the catalyst surface, particularly in micropores. Consequently, the incorporation of mesoporous structures into microporous catalyst supports, particularly those featuring hierarchical mesopores, may prove advantageous for catalysis under NTP conditions (Wang et al., 2022). This structural arrangement enhances the diffusion of plasma-generated reactive species, thereby improving the overall catalytic performance.

In this study, non-porous silicon dioxide and siliceous silicalite-1 zeolites with different pore structures, namely microporous and desilicated hierarchical meso-micro-porous silicalite-1, were synthesised and employed as supports for Pt nanoparticles. These catalysts were subjected to a comparative investigation of NTP-assisted chlorobenzene degradation. The primary objective was to elucidate the influence of pore structure on chlorobenzene degradation, by-products formation, PCDD/Fs generation.

2. Experimental

2.1. Preparation of catalysts

2.1.1. Preparation of microporous silicalite-1 (S1)

The catalyst synthesis procedure, as detailed by Xu et al. (2022), involved the gradual addition of 16.64 g of tetraethyl orthosilicate (TEOS, Sigma-Aldrich, ≥99.0%) to a 16.25 g solution of tetrapropylammonium hydroxide (TPAOH, Sigma-Aldrich, 1.0 M in H$_2$O), and 50 g H$_2$O under continuous stirring in a beaker. The resulting mixture was stirred for 6 h and subsequently subjected to heating in a Teflon-lined stainless-steel autoclave at 170 °C for a duration of 72 h. Following this synthesis period, the solid product was separated from the liquid phase through centrifugation, washed multiple times with deionised (DI) water, dried at 100 °C overnight, and calcined in a muffle furnace for 8 h at 550 °C.

2.1.2. Preparation of desilicated silicalite-1 (D-S1)

Cetyltrimethylammonium bromide (0.7 g) (CTAB, Fisher Scientific, Pure) was added into a beaker containing 50 mL of a dilute aqueous ammonia solution (NH$_4$OH, Merck, 15%). The mixture was stirred until complete dissolution of the surfactant. Subsequently, 1.0 g of the as-synthesised S1 was added to the solution and stirred for 3 h at room temperature. The resulting mixture was then transferred into an autoclave and heated at 90 °C for a duration of 24 h. Following this process, the solid product was separated from the liquid through centrifugation and washed with DI water. After drying the product overnight at 80 °C, the final powder was calcined in a muffle furnace at 550 °C for 10 h.

2.1.3. Preparation of Pt catalysts

Pt/S1 catalysts were synthesised employing a conventional incipient wetness impregnation method, with variations in the theoretical Pt loading at 0.5, 1.0, and 1.5 wt%, respectively. In detail, S1 was impregnated with a chloroplatinic acid hexahydrate ($H_2PtCl_6 \cdot 6H_2O$, Merck, $\geq 37.50\%$ Pt basis) aqueous solution for 12 h, followed by drying at 80 °C. Subsequently, the resulting solids underwent calcination in a muffle furnace at 500 °C for 4 h. Following the calcination step, the powder was reduced under a flow of H_2 (5% H_2 in nitrogen) at 50 sccm for a duration of 3 h at 450 °C, with a heating ramp of 5 °C min^{-1}. The nomenclature of the catalysts was determined based on the theoretical Pt wt% loading, denoted as xPt/S1 (x = 0.5, 1.0, and 1.5 respectively). The results of NTP assisted catalysis indicated that the 1.0 Pt/S1 outperformed all the other catalysts. For comparison, 1.0Pt/D-S1 catalysts and reference-supported Pt catalysts (1.0Pt/SiO$_2$) were also prepared with the same method to investigate the effects of supports structure on the chlorobenzene degradation and by-products formation.

2.2. Characterisation of materials

The catalysts underwent a comprehensive characterisation to elucidate their physical and chemical properties. The crystal structure of the zeolites was determined using X-ray diffraction (XRD) on a Bruker D8 diffractometer with Cu Kα radiation (40 kV and 40 mA). The scanning range was 5°–55° with a step size of 0.02°. Elemental analysis of the prepared catalysts was performed using a Varian Fast Sequential Atomic Absorption Spectrophotometer (AAS, AA204FS). Prior to AAS elemental analysis, the samples (~50 mg) were mixed with 12 mL aqua regia and digested for 30 min at 220 °C. H_2 pulse chemisorption was carried out by Micromeritics AutoChem II 2920 instrument to measure the Pt dispersion and active Pt surface areas. The samples were reduced at 300 °C for 1 h under 10% H_2/Ar flow (30 mL min^{-1}) and then were cooled down to 50 °C. The H_2 pulse chemisorption was then carried out by pulsing of a mixture of 10% H_2/Ar (30 mL min^{-1}). N_2 physisorption analysis of samples was carried out using a Micrometric Tristar 3000 Analyser. Prior to N_2 physisorption measurements, the samples (~50 mg) were degassed at 150 °C under N_2 atmosphere overnight. The Brunauer-Emmett-Teller (BET) method was employed to determine the specific surface area of materials. Scanning electron microscopy (SEM) images of the catalysts were obtained using Carl Zeiss EVO MA15 SEM with a high voltage mode of 20 kV. High-resolution transmission electron microscopy (HRTEM) images were collected with FEI Titan Cubed Themis 300 G2 FEG STEM operated at 200 kV, and energy dispersive X-ray spectroscopy (EDS) for element mapping was also carried out using an Oxford Ultim® Max system. The sample was prepared by dispersion of the powder catalysts in ethanol with the assistance of sonication, and a drop of the suspension was spread onto a TEM copper grid.

2.3. Chlorobenzene degradation and by-products analysis experiments

Fig. 1 illustrates the experimental setup. Chlorobenzene was injected into an evaporator by a syringe pump (KD Scientific, SPLG 100) with a rate of 0.05 g/h. The temperature of the evaporator was controlled by a tube furnace at 150 °C to ensure complete vaporisation of the feedstock. The carrier gas (Air) was regulated by a mass flow controller (Bronkhorst) at 50 mLmin^{-1}, facilitating the introduction of vaporised chlorobenzene into a continuous-flow dielectric barrier discharge (DBD) plasma reactor at atmospheric pressure, without an external heat source. The DBD plasma reactor consists of a cylindrical quartz reactor (6 mm O.D. × 4 mm I.D.), a stainless-steel rod (1 mm O.D., is used as the ground electrode and positioned along the axis of the quartz cylinder), and an aluminium foil sheet (functioning as a high voltage electrode) wrapped around the outer surface of the quartz reactor. The discharge length and gap of the DBD reactor were 10 and 1.5 mm, respectively. In a typical
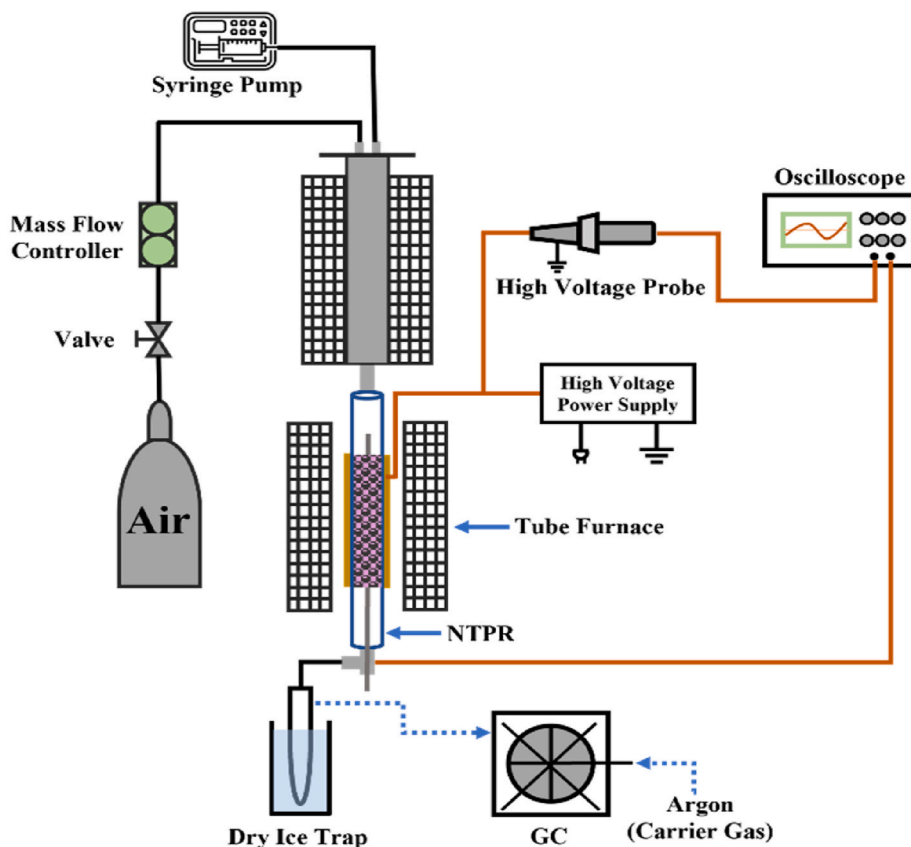
Fig. 1. Schematic diagram of the system for NTP assisted chlorobenzene catalytic degradation.

experiment, 100 mg of the synthesised catalyst (Pt/S1, Pt/D-S1, and Pt/SiO$_2$) were packed in the discharge zone between the ground electrode and the quartz reactor body. Throughout the reaction, the applied peak voltage was adjusted between 7.5 and 15.0 kV, maintaining a constant frequency of 20.3 kHz to investigate its impact on the chlorobenzene degradation. The applied peak voltage was measured using a digital oscilloscope (Tektronix MDO3024). The gases exiting the reactor were directed through a condenser cooled by a dry ice bath to facilitate the condensation of any vapours generated by the reaction. Following this, the gas chromatographs (GC, Varian-3800) were employed to analyse any remaining incondensable gases. The liquid collected from the dry ice bath was diluted with dichloromethane and analysed using the gas chromatographs-mass spectrometry (GC-MS, Varian-3800/-Saturn, 2000). The analysis of PCDD/Fs was undertaken by the Institute for Thermal Power Engineering, Zhejiang University, Hangzhou, China. The analytical procedure was based on the US Environmental Protection Agency Method 1613 and involved high resolution gas chromatography coupled with high resolution mass spectrometry (HRGC-HRMS) (JMS-800D, JEOL, Japan) with a DB-5MS column.

For the NTP assisted chlorobenzene degradation, chlorobenzene (X$_{CB}$, %) conversion was calculated using Eq. (1):

$$X_{CB} = \frac{n_{CB}^{in} - n_{CB}^{out}}{n_{CB}^{in}} \times 100\% \tag{1}$$

Where n$_{CB}^{in}$ and n$_{CB}^{out}$ are the mole of chlorobenzene in the inlet and outlet of the reactor, respectively.

The selectivity to CO (S$_{CO}$, %), CO$_2$ (S$_{CO_2}$, %) and CO$_x$ (S$_{CO_x}$, %) were calculated using Eq. (2), Eq. (3) and Eq. (4).

$$S_{CO} = \frac{n(CO)}{\left(n_{CB}^{in} - n_{CB}^{out}\right) \times 6} \times 100\% \tag{2}$$

$$S_{CO_2} = \frac{n(CO_2)}{\left(n_{CB}^{in} - n_{CB}^{out}\right) \times 6} \times 100\% \tag{3}$$

$$S_{CO_x} = \frac{n(CO) + n(CO_2)}{\left(n_{CB}^{in} - n_{CB}^{out}\right) \times 6} \times 100\% \tag{4}$$

The specific input energy (SIE, J mL^{-1}) was calculated using Eq. (5).

$$SIE = \frac{Power_{DBD}}{F_{Total}} \times 100\% \tag{5}$$

Where Power$_{DBD}$ is the power of the DBD plasma, and the F$_{Total}$ is the total flow rate of the catalytic system.

3. Results and discussion

3.1. Characterisation of catalysts

In Fig. 2a, the powder XRD patterns of S1, D-S1, and four Pt catalysts supported on various siliceous zeolites are presented. Characteristic peaks at 2θ = 7.97°, 8.83°, 23.17°, 24.09°, and 24.48° (highlighted in the shaded area) were observed for all zeolites and catalysts. These peaks confirm the well-crystallised MFI structure and the intactness of structure after impregnation (Niu et al., 2020). Alongside the strong diffraction peak of the zeolites, diffraction peaks associated with Pt at 2θ = 39.71° and 46.21° (highlighted in the shaded area), corresponding to the (111) and (200) facets, were observed for all Pt catalysts. This observation indicates the successful incorporation of Pt into the zeolite framework (Jiang et al., 2024). Furthermore, the intensity of diffraction peaks related to Pt in Pt/D-S1 catalysts was notably lower than in the other catalysts. This suggests the potential presence of highly dispersed small Pt particles on the support, or some Pt Nanoparticles may be encapsulated within the zeolites structure, likely promoted by the hierarchical mesoporous structure of D-S1 (Goodarzi et al., 2018).

SEM analysis of the different Pt catalysts supported on S1, D-S1, and SiO$_2$ is illustrated in Fig. S1. The images reveal that the ellipsoid-shape morphology of Pt/S1 and Pt/D-S1, and the crystal size are approximately between 0.5 and 1.0 μm. In contrast, the Pt catalysts supported on commercial SiO$_2$ exhibit significantly bigger particle sizes, approximately around 20 μm.

N$_2$ physisorption was carried out to investigate the relevant porous properties of the three different supports, and the results are presented in Table 1. The D-S1 exhibited the highest specific surface area (i.e. 388 m^2 g^{-1}), which could be contribute to mesopores formed by the desilication treatment. In the contrast, specific surface area of the SiO$_2$ was only 2.18 m^2 g^{-1} due to its dense and compact structure. The N$_2$ adsorption-desorption isotherms of S1 and D-S1 are shown in Fig. S2.
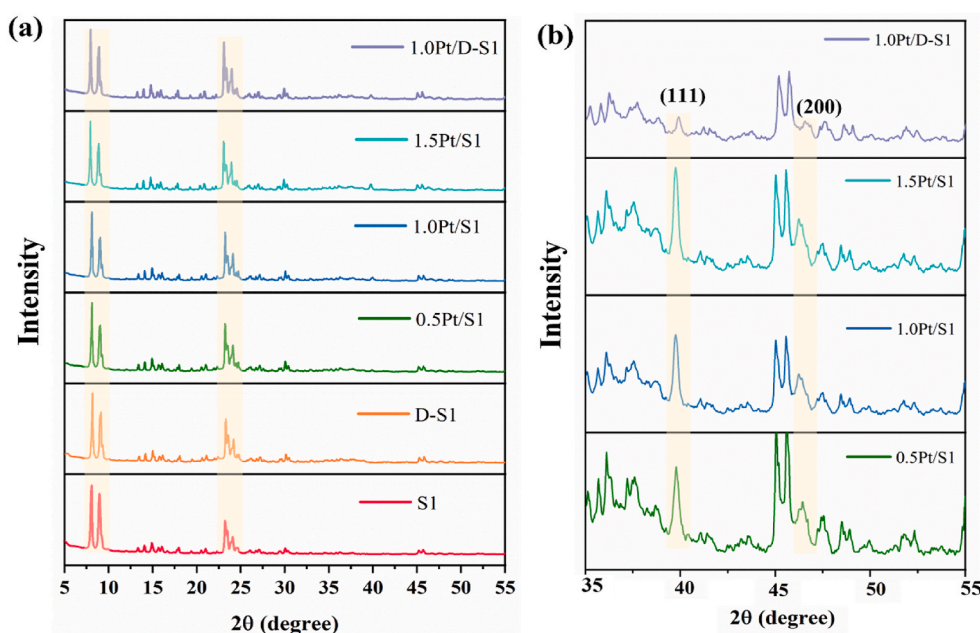
Fig. 2. XRD patterns of the microporous silicalite-1 (S1) and desilicated silicalite-1 (D-S1) supports and as-prepared catalysts (after calcination in air at 550 °C).

Table 1
Porous properties of different supports by N_2 physisorption analysis.

Materials	S_{BET} ($m^2 g^{-1}$)	V_{total} ($cm^3 g^{-1}$)	V_{micro} ($cm^3 g^{-1}$)	V_{meso} ($cm^3 g^{-1}$)
SiO_2	2.19	–	–	–
S1	347	0.184	0.121	0.063
D-S1	388	0.227	0.094	0.133

Both of the S1 and DS1 exhibited a steep increase in the N_2 uptake at low relative pressure ($P/P_0 < 0.01$) due to micropores being filled by N_2 molecules, confirming the presence of microporous structure regardless of their structure. Additionally, the isotherm of D-S1 showed the H4 hysteresis loop that is at around $P/P_0 = 0.45$, indicating the presence of mesoporous structures in the zeolites.

Detailed information about the dispersion and size of Pt nanoparticles in the different supports was further investigated by HRTEM. As shown in Fig. 3a to 5c, for the 1Pt/SiO₂ catalysts, large and irregularly agglomerated Ni particles are mainly formed on the external surface of SiO₂, with an average particle size of 13.18 nm. In contrast, for the 1 Pt/S1 catalysts, the distribution of the Pt nanoparticles is significantly better than that observed in the Pt/SiO₂ catalysts, with less agglomeration of Pt nanoparticles. In addition, the average particle size of Pt nanoparticles (~9.8 nm) is also smaller in the 1 Pt/S1 catalysts compared to the 1Pt/SiO₂ catalysts. The enhanced dispersion of Pt nanoparticles in the 1 Pt/S1 catalysts can be attributed to the porous structure of the zeolite supports (Sun et al., 2021). The larger surface area and uniform pore size contribute to a more controllable distribution of the metal during the synthesis of catalysts. For the 1Pt/D-S1 catalysts with the hierarchical meso-micro-porous structure promoted the formation of very small Pt nanoparticles with a particle size approximately at 6.19 nm as shown in Fig. 3i to 5k. This is in accordance with the findings of XRD, where the characteristic peak of Pt in 1Pt/D-S1 is much weaker than the peaks in the other two catalysts. Furthermore, by the cumulative frequency analysis as shown in Figs. 3d, 5h and 5l, it can be found that more than 90% of the Pt nanoparticles in 1Pt/D-S1 is smaller than 8.65 nm (d (90) = 8.65 nm) which is quite close to the mean particle size indicating a highly uniform Pt nanoparticles were deposited on the D-S1.

To visually analyse the dispersion of metals on different supports, TEM-EDS mapping and H_2 chemisorption were employed for further investigation. As shown in Fig. S3 (a) and (d), for the 1Pt/SiO₂ catalysts, the distribution of the Pt nanoparticles was uneven, mainly concentrated on the top of the SiO₂ support, with almost no Pt nanoparticles observed in the middle area of the support. Consequently, the H_2 chemisorption results (Table S1) indicated that Pt dispersion of the 1Pt/SiO₂ was the lowest among all the catalysts, measuring only 0.626%. For the 1 Pt/S1 catalysts, as shown in Fig. S3 (b) and (e), the Pt nanoparticles were evenly dispersed on the surface of the zeolites, resulting in a higher dispersion rate (i.e. 0.805%) compared to 1Pt/SiO₂. However, some agglomeration was also observed on the catalysts, which had a negative impact on the metal dispersion. The dispersion rate of 1Pt/D-S1 (i.e. 1.87%) outperformed all the other catalysts. From Fig. S3 (e) and (f), it could be found the Pt nanoparticles were evenly deposited on the D-S1 and no agglomeration were observed.

3.2. Catalytic degradation of chlorobenzene over the catalysts under NTP conditions

Fig. 4 presents the relevant results of NTP assisted catalytic degradation of chlorobenzene in different systems, namely catalyst-free, with the Pt/SiO₂, Pt/S-1, and Pt/DS-1 packing, respectively. In the catalyst-free NTP system, chlorobenzene degradation conversion was relatively low, ranging from ca., 25%–48%, compared to the catalysts packing system. However, with increasing input energy, around half of the input chlorobenzene was still eliminated in the NTP system at 37 J mL⁻¹. This can be attributed to the active species generated by the NTP, such as vibrationally-excited molecules, radicals, atoms and ions which can enhance the breakdown of the chemical bonds in the chlorobenzene (Kim et al., 2016; Chen et al., 2020c). Nevertheless, as shown in Fig. 4b, the CO_x selectivity in the catalyst-free NTP system was extremely low. This can be explained by the high energy from the above-mentioned active species mainly destroyed the benzene ring to generate reactive species such as methyl and phenyl radicals (Jiang et al., 2021; Zhao et al., 2023). These intermediates are subsequently oxidised to various
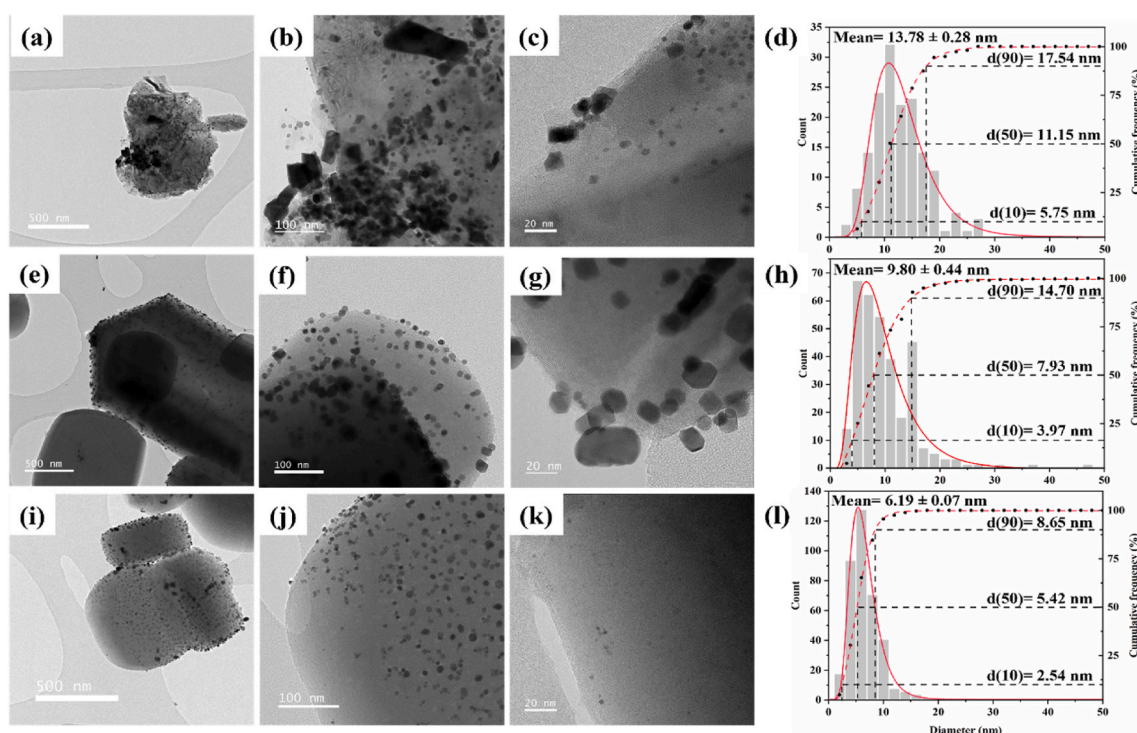
Fig. 3. HRTEM images and corresponding Pt particle size distribution of (a–d) 1Pt/SiO₂, (e–h) 1 Pt/S1 and (i–l) 1Pt/D-S1.
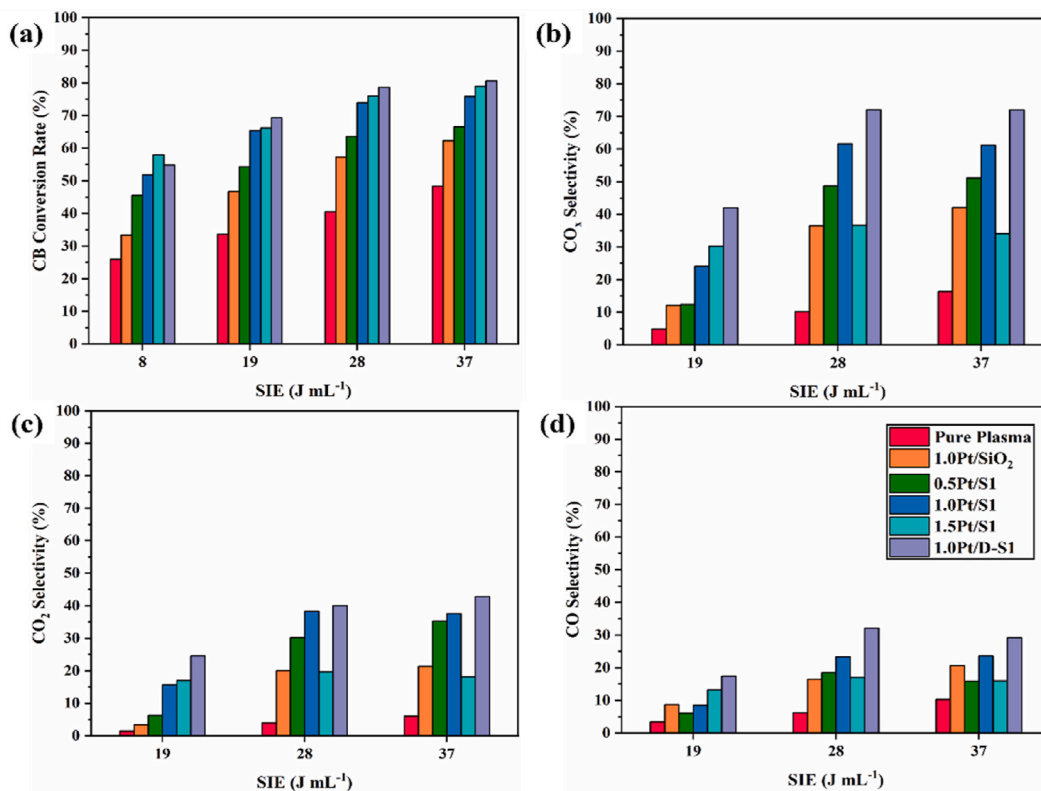
Fig. 4. NTP assited catalytic chlorobenzene degradation performance over the pure NTP condition, Pt/S1, Pt/D-S1, and Pt/SiO₂: (a) chlorobenzene conversion rate, (b) CO_x selectivity, (c) CO_2 Selectivity and (d) CO selectivity (experiment conditions: carrier gas flow rate of 50 sccm, chlorobenzene inlet speed of 0.05 g/h, applied voltage of 7.5 kV–15 kV, the specific input energy (SIE) was calculated by using Eq. (5)).
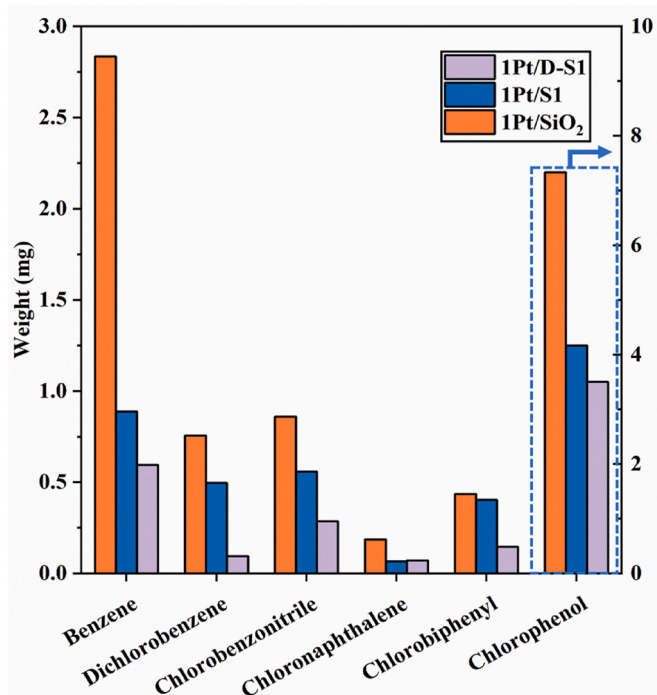
Fig. 5. Main organic by-products formed in the NTP assisted catalytic chlorobenzene degradation over different catalysts (experiment conditions: carrier gas flow rate of 50 sccm, chlorobenzene inlet speed of 0.05 g/h, applied voltage of 12.5 kV).

by-products including Ethyl acetate, ethylene oxide, propyne and ketene (Liang et al., 2021; Mu and Williams, 2022). Only a very small amount of intermediates can be fully oxidised into the desired CO_x, primarily CO.

All NTP systems involving catalysts outperformed the NTP-only system in both chlorobenzene conversion rate and CO_x selectivity. However, under 8 J mL^{-1}, CO and CO_2 were undetectable in all systems, indicating insufficient energy to activate the catalysts. Among the various catalysts, the Pt/S-1 catalysts exhibited better catalytic performance than Pt/SiO₂ in both chlorobenzene conversion rate and CO_x selectivity, suggesting a promotion effect by S1 and D-S1 (as the supports to promote the dispersion of Pt phase and Pt nanoparticle size). This is confirmed by the above-mentioned findings of HRTEM results and H₂ pulse chemisorption analysis, which showed significantly higher Pt dispersion in the Pt/S1 catalysts (e.g., about 1.87% for 1Pt/D-S1) than that of 1Pt/SiO₂ (ca., 0.626%). An increase in Pt loading was found to be beneficial to the degradation of chlorobenzene. For example, at 37 J mL^{-1}, the 1.5 Pt/S1 demonstrated the highest chlorobenzene conversion rate of ca. 78%. However, the 1.5 Pt/S1 presented a relatively poor selectivity of CO_x under a high SIE(ca., 36% under 28 J mL^{-1}). This may be attributed to the agglomeration of Pt nanoparticles on the surface of S1 due to the overloading of Pt. The agglomeration of Pt resulted in a decrease in the utilisation rate of Pt nanoparticles. As a result, under high SIE, there may have insufficient Pt nanoparticles can interact with the active species generated by the NTP. Meanwhile, these active species directly interact with chlorobenzene, leading to a disordered and stochastic degradation reaction, resulting in low COx selectivity. Additionally, an increase in power was also found to be advantageous for the selective conversion of chlorobenzene. However, when the energy density reached 28 J mL^{-1}, the impact of increasing the energy density on the chlorobenzene degradation was minimal.

The 1Pt/D-S1 catalysts outperformed all the other catalysts, suggesting the desilication of the S1 have a great impact on the catalytic

performance in the NTP system. For example, at 28 J mL^{-1}, the 1Pt/D-S1 presented the highest chlorobenzene conversion rate and CO$_x$ selectivity, which were 80% and 75%, respectively. This can be explained by (i) the high dispersion of small Pt nanoparticles in the Pt/D-S1 catalysts (as shown in), (ii) the improved diffusivity of chlorobenzene and gaseous reactants into the pores of zeolite supports, and (iii) the formation of microdischarges in the NTP system which was of the order, D-S1>S1>SiO$_2$. In section 3.1, a detailed discussion was provided on how the hierarchical meso-micro-porous structure of D-S1 impacted metal dispersion and nanoparticles size, consequently influencing the utilisation efficiency of metal in the catalytic reaction. It is also well recognised that larger pore size is advantageous for facilitating better diffusion of molecules. In this case, the larger pore size allowed chlorobenzene molecules to more efficiently reach the active sites of Pt-based catalysts, as well as the active reactants generated by the NTP (Zhao et al., 2014; Li et al., 2015; Gao et al., 2023). Furthermore, the mesopores present in the zeolites can contribute to microdischarge formation, increase in electric field, and enhancement of electron density in the NTP system (Zhang et al., 2016, 2017; Yao et al., 2018). This resulted in the generation of more active reactants, thereby enhancing the degradation performance of chlorobenzene.

3.3. Organic by-products analysis and the distribution of PCDDs and PCDFs

To investigate the formation of organic by-products in the NTP-assisted catalytic degradation process, all organic compounds were condensed using dry ice and identified using the GC-MS. Based on the different retention times of compounds observed in the total ion chromatogram, the NIST 2000 spectrum library database was utilised to classify the compounds into their respective categories. The main substances formed by different catalysts (including 1Pt/SiO$_2$, 1 Pt/S1 and 1Pt/D-S1) under the SIE of 28 J mL^{-1} are summarised in Table S2.

The 1Pt/SiO$_2$ catalysts generated the highest number of organic compounds, totalling 18 different species, whereas only 12 organic by-products were identified in the condensate from the 1Pt/D-S1 catalytic system. Among the 3 catalyst systems, 6 different types of benzene and its chlorinated derivatives were all detected in the condensate, including benzene, dichlorobenzene, chlorobenzonitrile, chloronaphthalene, chlorobiphenyl, and chlorophenol. The 1Pt/SiO$_2$ catalysts formed the highest amount of benzene (ca., 2.8 mg) as shown in Fig. 5, which was around 5 times higher than the benzene formed from 1Pt/D-S1. Benzene is generally considered to be more toxic than chlorobenzene and is classified as a Group 1 carcinogen by the IARC (Henschler, 1994; Fletcher et al., 2002). Therefore, in NTP-assisted Cl–VOCs degradation, it is crucial to consider the potential for inhibiting the formation of more toxic by-products. Minimising the production of benzene and other highly toxic compounds is essential to ensure the safety and effectiveness of the degradation process. The reasons why 1Pt/D-S1 formed the lowest benzene can be attributed to the hierarchical meso-micro-porous structure of D-S1. Regarding the chlorobenzene molecule, the bond energy of the C–Cl bond in its branched chain (4.2 eV) is lower than that of the C–H bond (4.4 eV), C–C bond (5.0–5.3 eV), and C=C bond (5.5 eV) (Li et al., 2021a; Zhou et al., 2021; Xie et al., 2022). Therefore, during the discharge process, the C–Cl bond in the chlorobenzene molecule is likely to break first to form a Cl atom and a phenyl radical (as shown in Eq. (6)). Subsequently, the benzene ring may undergo ring-opening reactions under the dual action of active free radicals and high-energy electrons.

$$C_6H_5Cl + e \rightarrow C_6H_5 \cdot + Cl \tag{6}$$

As discussed previously, the hierarchical structure of D-S1 can enhance the microdischarges in the NTP system. The presence of microdischarges typically indicates a higher electron density which can provide sufficient energy to break the C–H bond, C–C bond and C=C bond after breaking the C–Cl bond. Additionally, the mesopores present

in the 1Pt/D-S1 catalyst facilitated the rapid diffusion of short-lived reactive species generated by the NTP to the metal active sites. This enhanced diffusion proved to be beneficial for the deep oxidation of chlorobenzene. Furthermore, the enhanced adsorption ability and larger specific surface area of the zeolite catalysts may also contribute to the deep oxidation of Cl–VOCs. Zeolite can efficiently adsorb reactants onto catalysts and interact with the reactive metal sites, thereby facilitating the selective and deep oxidation of chlorobenzene while attempting to prevent dissociation or self-/cross-coupling of chlorobenzene and other dissociated organic compounds, which are directly influenced by the plasma rather than the metal catalysts.

In addition to benzene, dichlorobenzene was also found as a main organic by-product in the GC-MS analysis. The quantity of dichlorobenzene generated by 1Pt/SiO$_2$ (ca., 0.756 mg) was significantly higher compared to the 1 Pt/S1 and 1Pt/D-S1, which formed 0.496 mg and 0.094 mg dichlorobenzene, respectively. The formation of dichlorobenzene is believed to be the result of the Cl atom formed in Eq. (6) which can further react with the chlorobenzene via the positioning law of the electrophilic substitution reaction on the aromatic ring (Zhu et al., 2024). Interestingly, all three possible structural isomers of dichlorobenzene (including 1,2-dichlorobenzene, 1,3-dichlorobenzene, and 1,4-dichlorobenzene) were identified on all the catalysts. However, 1,2-dichlorobenzene was the dominant structure detected from 1Pt/SiO$_2$. The relatively higher formation energy is required of 1,4-dichlorobenzene due to the para position of two chlorine atoms, which can lead to steric hindrance and repulsion between the chlorine atoms (Deng et al., 2020). As discussed earlier, it was noted that the microdischarge and electron density of the 1Pt/SiO$_2$ system were lower compared to the other two catalysts. Consequently, this condition favoured the formation of 1,2-dichlorobenzene, as it required less energy for its formation compared to other isomers.

Dioxin-like polychlorinated biphenyl and many other chlorinated organic compounds which have potential to form highly toxic dioxins such as chlorophenol (Evans and Dellinger, 2005; Peng et al., 2016), dichlorophenol (Mosallanejad et al., 2016; Yang et al., 2017a), chloronaphthalene (Ghorishi and Altwicker, 1996; Mosallanejad et al., 2016), and chlorobenzonitrile (Kuzuhara et al., 2005; Fu et al., 2015) were also detected in the GC-MS analysis. Herein, the used catalysts were further investigated by high-resolution gas chromatography-high resolution mass spectrometry (HRGC-HRMS) to identify and quantify the PCDDs and PCDFs formed on the catalysts.

Based on the research findings from conventional thermal catalysis, the temperature window for dioxin formation typically ranges from 200 to 600 °C (Xiong et al., 2022). In the NTP system, temperature is maintained below 200 °C, suggesting that the formation of PCDD/Fs may be less likely. However, the results from HRGC/HRMS results indicated that the PCDD/Fs formation was inevitable in the NTP assisted catalytic system. All 17 types of PCDD/Fs were detected on the three catalysts. Fig. 6 presents the measured value and toxic equivalent (TEQ) of 17 different PCDD/Fs formed on the three catalysts. The TEQ uses the available toxicological and biological data to generate a set of weighting factors each of which expresses the toxicity of a particular PCDD or PCDF congener in terms of an equivalent amount of 2,3,7,8 TCDD. Indeed, in conventional thermal conditions, exceeding the temperature window aims to promote the dissociation of oxygen, crucial for the formation of active oxygen species involved in PCDD/Fs formation (Yu et al., 2022). However, in NTP systems, various oxygen species can be generated even at near-room temperature in the presence of oxygen. As a result, the 1Pt/D-S1 showed apparently lower PCDD/Fs concentrations than the other two catalysts. The total toxic equivalent of 1Pt/SiO$_2$ (25,100 ng TEQ kg^{-1}) was about 68 times that of 1Pt/D-S1 (367 ng TEQ kg^{-1}). This finding was consistence with the result from GC-MS as shown in Fig. 5, where 1Pt/SiO$_2$ formed the highest amount of chlorophenol (ca., 7.2 mg), known as direct precursors of PCDD/Fs formation, while only 3.5 mg chlorophenol was formed by the 1Pt/D-S1 catalysts (Pan et al., 2013).
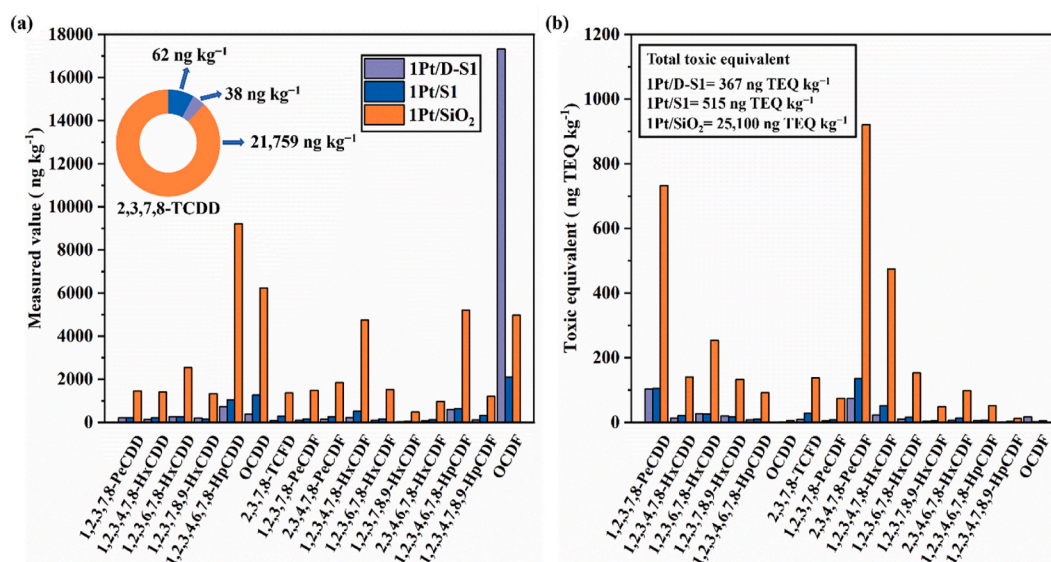
Fig. 6. Measured value and toxity equivalent of 17 different PCDDs and PCDFs formed from the NTP assisted degradation of chlorobenzene over different catalysts (1Pt/SiO₂, 1 Pt/S1 and 1Pt/D-S1).

It is believed that both Langmuir-Hinshelwood and Eley–Rideal mechanisms coexist in the NTP system, both of which require the adsorption of molecules on the catalysts (Chen et al., 2019). Pore size plays an important role in the adsorption of VOCs (Li et al., 2020). The non-porous structure of SiO₂, with a flat or nearly featureless surface, results in poor adsorption performance for chlorobenzene. Therefore, many chlorobenzene molecules were not able to adsorb onto the catalysts and instead reacted with them, resulting in higher formation of chlorinated organic by-products and PCDD/Fs. Furthermore, Yu et al. (2022) investigated plasma-catalysis for the abetment of chlorobenzene and found that PCDD/Fs could only be detected after a discharge time of 10 h, indicating that the formation of PCDD/Fs required the concentration of precursors to accumulate on the catalyst surface to a certain extent. Therefore, rapid transportation of intermediates without participating in the chlorination process is a crucial strategy. The micropore structure of S1, restricted the movement of gas molecules and intermediates between surfaces, resulting in slower diffusion rates and the accumulation of chlorinated-related intermediates (Wang et al., 2023). On the other hand, the hierarchical structures in 1Pt/D-S1can significantly enhance the mass transfer rate which accelerate transformation of intermediates and reduce the possibility of self-/-cross-coupling reactions of dioxins precursors, such as chlorophenol and dichlorophenol resulting in a lower total toxic equivalent (Li et al., 2021c). This helps to explain why 3,4-dichlorophenol could only be detected from the 1Pt/SiO₂ as shown in Table S2.

4. Conclusions

In NTP assisted catalytic degradation of chlorobenzene, minimising the production of highly toxic by-products, and achieving the deep oxidation of chlorobenzene is a major challenge. In this study, a series of Pt nanoparticles supported on SiO₂, microporous silicalite-1 (S1) and desilicated silicalite-1 (D-S1) catalysts were investigated. Comprehensive characterisation of the catalysts revealed the influence of pore structure on metal size and dispersion rate, with Pt/D-S1 exhibiting the smallest particle size (~6.19 nm) and the highest dispersion rate (~1.87). This resulted in superior catalytic performance, with Pt/D-S1 achieving the highest chlorobenzene conversion and COx selectivity at approximately 80% and 75%, respectively.

The pore structure also affected the formation of by-products, with Pt/SiO₂ generating a greater variety of organic compounds compared to

Pt/D-S1. Specifically, the amount of benzene produced by Pt/SiO2 was observed to be 100 times greater than that generated by Pt/D-S1. A similar trend was noted in the formation of chlorophenol across different catalysts. All catalysts yielded polychlorinated biphenyls and other chlorinated organic compounds which were precursors in dioxins formation, indicating the unavoidable formation of PCDD/Fs in the NTP-assisted catalytic system. However, Pt/D-S1 showed lower PCDD/Fs concentrations and reduced formation of chlorophenol, a precursor to PCDD/Fs, compared to other catalysts. The hierarchical structure of D-S1 facilitated microdischarges in the NTP system, enhancing electron density and diffusion rates, thereby aiding in chlorobenzene degradation and minimising toxic by-product formation. Furthermore, rapid transportation of intermediates without participating in chlorination processes proved crucial in reducing PCDD/Fs formation, highlighting the importance of catalyst structure in inhibiting toxic by-products.

This work aimed to understand the significance of synthesis-structure-performance correlations in catalyst design for efficient chlorinated volatile organic compound degradation in NTP systems. Its findings offer valuable insights for future research and development in environmental remediation strategies.

CRediT authorship contribution statement

Yibing Mu: Writing – original draft, Methodology, Investigation, Conceptualization. **Yilai Jiao:** Investigation. **Xinrui Wang:** Investigation. **Paul T. Williams:** Writing – review & editing, Supervision, Funding acquisition, Conceptualization.

Declaration of competing interest

The authors declare that they have no known competing financial interests or personal relationships that could have appeared to influence the work reported in this paper.

Data availability

Data will be made available on request.

Appendix A. Supplementary data

Supplementary data to this article can be found online at https://doi.org/10.1016/j.chemosphere.2024.142294.

References

Abedi, K.A.-D., Ghorbani-Shahna, F., Bahrami, A., Ebrahimi, H., Maleki, A., Madjidi, F., Musavi, S., Mohammadi, E., Giahi, O., 2018. Effect of TiO2/GAC and water vapor on chloroform decomposition in a hybrid plasma-catalytic system. Environ. Technol. 39, 2041–2050.

Altarawneh, M., Dlugogorski, B.Z., Kennedy, E.M., Mackie, J.C., 2009. Mechanisms for formation, chlorination, dechlorination and destruction of polychlorinated dibenzo-p-dioxins and dibenzofurans (PCDD/Fs). Prog. Energy Combust. Sci. 35, 245–274.

Chen, H., Goodarzi, F., Mu, Y., Chansai, S., Mielby, J.J., Mao, B., Sooknoi, T., Hardacre, C., Kegnæs, S., Fan, X., 2020a. Effect of metal dispersion and support structure of Ni/silicalite-1 catalysts on non-thermal plasma (NTP) activated CO2 hydrogenation. Appl. Catal., B 272, 119013.

Chen, H., Mu, Y., Shao, Y., Chansai, S., Xiang, H., Jiao, Y., Hardacre, C., Fan, X., 2020b. Nonthermal plasma (NTP) activated metal–organic frameworks (MOFs) catalyst for catalytic CO2 hydrogenation. AIChE J. 66, e16853.

Chen, H., Mu, Y., Shao, Y., Chansai, S., Xu, S., Stere, C.E., Xiang, H., Zhang, R., Jiao, Y., Hardacre, C., 2019. Coupling non-thermal plasma with Ni catalysts supported on BETA zeolite for catalytic CO 2 methanation. Catal. Sci. Technol. 9, 4135–4145.

Chen, H., Mu, Y., Xu, S., Xu, S., Hardacre, C., Fan, X., 2020c. Recent advances in non-thermal plasma (NTP) catalysis towards C1 chemistry. Chin. J. Chem. Eng. 28, 2010–2021.

Chen, H., Shao, Y., Mu, Y., Xiang, H., Zhang, R., Chang, Y., Hardacre, C., Wattanakit, C., Jiao, Y., Fan, X., 2021. Structured silicalite-1 encapsulated Ni catalyst supported on SiC foam for dry reforming of methane. AIChE J. 67, e17126.

Choi, M.S., Qiu, X., Zhang, J., Wang, S., Li, X., Sun, Y., Chen, J., Ying, Q., 2020. Study of secondary organic aerosol formation from chlorine radical-initiated oxidation of volatile organic compounds in a polluted atmosphere using a 3D chemical transport model. Environ. Sci. Technol. 54, 13409–13418.

Deng, W., Tang, Q., Huang, S., Zhang, L., Jia, Z., Guo, L., 2020. Low temperature catalytic combustion of chlorobenzene over cobalt based mixed oxides derived from layered double hydroxides. Appl. Catal., B 278, 119336.

Epa, U., 2014. Appendix A to 40 CFR, Part 423–126 Priority Pollutants.

Evans, C.S., Dellinger, B., 2005. Mechanisms of dioxin formation from the high-temperature oxidation of 2-chlorophenol. Environ. Sci. Technol. 39, 122–127.

Fletcher, C.D., Unni, K., Mertens, F., 2002. World Health Organization Classification of Tumours. Pathology and Genetics of Tumours of Soft Tissue and Bone. IARC press.

Fu, J.-Y., Li, X.-D., Chen, T., Lin, X.-Q., Buekens, A., Lu, S.-Y., Yan, J.-H., Cen, K.-F., 2015. PCDD/Fs' suppression by sulfur–amine/ammonium compounds. Chemosphere 123, 9–16.

Gao, W., Tang, X., Yi, H., Jiang, S., Yu, Q., Xie, X., Zhuang, R., 2023. Mesoporous molecular sieve-based materials for catalytic oxidation of VOC: a review. J. Environ. Sci. 125, 112–134.

García-Martínez, J., Johnson, M., Valla, J., Li, K., Ying, J.Y., 2012. Mesostructured zeolite Y—high hydrothermal stability and superior FCC catalytic performance. Catal. Sci. Technol. 2, 987–994.

Ghorishi, S.B., Altwicker, E.R., 1996. Rapid formation of polychlorinated dioxins/furans during the heterogeneous combustion of 1, 2-dichlorobenzene and 2, 4-dichlorophenol. Chemosphere 32, 133–144.

Goodarzi, F., Kang, L., Wang, F.R., Joensen, F., Kegnæs, S., Mielby, J., 2018. Methanation of carbon dioxide over zeolite-encapsulated Nickel nanoparticles. ChemCatChem 10, 1566–1570.

Henschler, D., 1994. Toxicity of chlorinated organic compounds: effects of the introduction of chlorine in organic molecules. Angew. Chem. Int. Ed. 33, 1920–1935.

Jiang, N., Li, X., Kong, X., Zhao, Y., Li, J., Shang, K., Lu, N., Wu, Y., 2021. The post plasma-catalytic decomposition of toluene over K-modified OMS-2 catalysts at ambient temperature: effect of K+ loading amount and reaction mechanism. J. Colloid Interface Sci. 598, 519–529.

Jiang, Y., Wang, Y., Qian, J., Mu, Y., Li, Z., Zhao, T., Zeng, L., 2024. Durable carbon-shell-encapsulated Pt/C catalysts synthesized by direct pyrolysis of Pt-pyrrole complexes for the oxygen reduction reaction. Int. J. Hydrogen Energy 51, 578–586.

Kim, H.-H., Teramoto, Y., Ogata, A., Takagi, H., Nanba, T., 2016. Plasma catalysis for environmental treatment and energy applications. Plasma Chem. Plasma Process. 36, 45–72.

Kuzuhara, S., Sato, H., Tsubouchi, N., Ohtsuka, Y., Kasai, E., 2005. Effect of nitrogen-containing compounds on polychlorinated dibenzo-p-dioxin/dibenzofuran formation through de novo synthesis. Environ. Sci. Technol. 39, 795–799.

Lei, C., Liang, F., Li, J., Chen, W., Huang, B., 2019. Electrochemical reductive dechlorination of chlorinated volatile organic compounds (Cl-VOCs): effects of molecular structure on the dehalogenation reactivity and mechanisms. Chem. Eng. J. 358, 1054–1064.

Li, L., Shi, J.-W., Tian, M., Chen, C., Wang, B., Ma, M., He, C., 2021a. In situ fabrication of robust three dimensional ordered macroporous γ-MnO2/LaMnO3. 15 catalyst for chlorobenzene efficient destruction. Appl. Catal., B 282, 119565.

Li, S., Yu, X., Dang, X., Meng, X., Zhang, Y., Qin, C., 2021b. Non-thermal plasma coupled with MOx/γ-Al2O3 (M: Fe, Co, Mn, Ce) for chlorobenzene degradation: analysis of byproducts and the reaction mechanism. J. Environ. Chem. Eng. 9, 106562.

Li, X., Wang, J., Guo, Y., Zhu, T., Xu, W., 2021c. Adsorption and desorption characteristics of hydrophobic hierarchical zeolites for the removal of volatile organic compounds. Chem. Eng. J. 411, 128558.

Li, X., Zhang, L., Yang, Z., Wang, P., Yan, Y., Ran, J., 2020. Adsorption materials for volatile organic compounds (VOCs) and the key factors for VOCs adsorption process: a review. Sep. Purif. Technol. 235, 116213.

Li, Y., Wang, H., Dong, M., Li, J., Qin, Z., Wang, J., Fan, W., 2015. Effect of zeolite pore structure on the diffusion and catalytic behaviors in the transalkylation of toluene with 1, 2, 4-trimethylbenzene. RSC Adv. 5, 66301–66310.

Liang, Y., Li, J., Xue, Y., Tan, T., Jiang, Z., He, Y., Shangguan, W., Yang, J., Pan, Y., 2021. Benzene decomposition by non-thermal plasma: a detailed mechanism study by synchrotron radiation photoionization mass spectrometry and theoretical calculations. J. Hazard Mater. 420, 126584.

Lin, F., Wang, Z., Zhang, Z., Xiang, L., Yuan, D., Yan, B., Wang, Z., Chen, G., 2021a. Comparative investigation on chlorobenzene oxidation by oxygen and ozone over a MnO x/Al2O3 catalyst in the presence of SO2. Environ. Sci. Technol. 55, 3341–3351.

Lin, F., Zhang, Z., Li, N., Yan, B., He, C., Hao, Z., Chen, G., 2021b. How to achieve complete elimination of Cl-VOCs: a critical review on byproducts formation and inhibition strategies during catalytic oxidation. Chem. Eng. J. 404, 126534.

Mosallanejad, S., Dlugogorski, B.Z., Kennedy, E.M., Stockenhuber, M., Lomnicki, S.M., Assaf, N.W., Altarawneh, M., 2016. Formation of PCDD/Fs in oxidation of 2-chlorophenol on neat silica surface. Environ. Sci. Technol. 50, 1412–1418.

Mu, Y., Williams, P.T., 2022. Recent advances in the abatement of volatile organic compounds (VOCs) and chlorinated-VOCs by non-thermal plasma technology: a review. Chemosphere 136481.

Niu, X., Li, X., Yuan, G., Feng, F., Wang, M., Zhang, X., Wang, Q., 2020. Hollow hierarchical silicalite-1 zeolite encapsulated PtNi bimetals for selective hydroconversion of methyl stearate into aviation fuel range alkanes. Ind. Eng. Chem. Res. 59, 8601–8611.

Pan, W., Zhang, D., Han, Z., Zhan, J., Liu, C., 2013. New insight into the formation mechanism of PCDD/Fs from 2-chlorophenol precursor. Environ. Sci. Technol. 47, 8489–8498.

Peng, Y., Chen, J., Lu, S., Huang, J., Zhang, M., Buekens, A., Li, X., Yan, J., 2016. Chlorophenols in municipal solid waste incineration: a review. Chem. Eng. J. 292, 398–414.

Sun, P., Long, Y., Long, Y., Cao, S., Weng, X., Wu, Z., 2020. Deactivation effects of Pb (II) and sulfur dioxide on a γ-MnO2 catalyst for combustion of chlorobenzene. J. Colloid Interface Sci. 559, 96–104.

Sun, Q., Wang, N., Yu, J., 2021. Advances in catalytic applications of zeolite-supported metal catalysts. Adv. Mater. 33, 2104442.

Wang, J., Shi, Y., Kong, F., Zhou, R., 2023. Low-temperature VOCs oxidation performance of Pt/zeolites catalysts with hierarchical pore structure. J. Environ. Sci. 124, 505–512.

Wang, T., Yang, C., Gao, P., Zhou, S., Li, S., Wang, H., Sun, Y., 2021. ZnZrOx integrated with chain-like nanocrystal HZSM-5 as efficient catalysts for aromatics synthesis from CO2 hydrogenation. Appl. Catal., B 286, 119929.

Wang, X., Xu, S., Yang, W., Fan, X., Pan, Q., Chen, H., 2022. Development of Ni-Co supported on SBA-15 catalysts for non-thermal plasma assisted co-conversion of CO2 and CH4: results and lessons learnt. Carbon Capture Sci. 5, 100067.

Weng, X., Meng, Q., Liu, J., Jiang, W., Pattisson, S., Wu, Z., 2018. Catalytic oxidation of chlorinated organics over lanthanide perovskites: effects of phosphoric acid etching and water vapor on chlorine desorption behavior. Environ. Sci. Technol. 53, 884–893.

Whalley, L.K., Slater, E.J., Woodward-Massey, R., Ye, C., Lee, J.D., Squires, F., Hopkins, J.R., Dunmore, R.E., Shaw, M., Hamilton, J.F., 2021. Evaluating the sensitivity of radical chemistry and ozone formation to ambient VOCs and NO x in Beijing. Atmos. Chem. Phys. 21, 2125–2147.

Xie, L., Lu, J., Ye, G., Yao, J., Zou, X., Zhu, C., 2022. Decomposition of gaseous chlorobenzene using a DBD combined CuO/α-Fe2O3 catalysis system. Environ. Technol. 43, 2743–2754.

Xiong, S., Yaqi, P., Shengyong, L., Chen, K., Li, X., Kefa, C., 2022. PCDD/Fs from a large-scale municipal solid waste incinerator under transient operations: insight formation pathways and optimal reduction strategies. J. Environ. Manage. 314, 114878.

Xu, S., Chen, H., Fan, X., 2023. Rational design of catalysts for non-thermal plasma (NTP) catalysis: a reflective review. Catal. Today, 114144.

Xu, S., Slater, T.J., Huang, H., Zhou, Y., Jiao, Y., Parlett, C.M., Guan, S., Chansai, S., Xu, S., Wang, X., 2022. Developing silicalite-1 encapsulated Ni nanoparticles as sintering-/coking-resistant catalysts for dry reforming of methane. J. Chem. Eng. 446, 137439.

Yang, Y., Liu, G., Zheng, M., Zhao, Y., Jin, R., Wu, X., Xu, Y., 2017a. Molecular mechanism of dioxin formation from chlorophenol based on electron paramagnetic resonance spectroscopy. Environ. Sci. Technol. 51, 4999–5007.

Yang, P., Zuo, S., Zhou, R., 2017b. Synergistic catalytic effect of (Ce, Cr) xO2 and HZSM-5 for elimination of chlorinated organic pollutants. J. Chem. Eng. 323, 160–170.

Yao, X., Zhang, J., Liang, X., Long, C., 2018. Plasma-catalytic removal of toluene over the supported manganese oxides in DBD reactor: effect of the structure of zeolites support. Chemosphere 208, 922–930.

Yeh, C.-H., Lin, W.-Y., Jiang, J.-C., 2020. Enhancement of chlorobenzene sensing by doping aluminum on nanotubes: a DFT study. Appl. Surf. Sci. 514, 145897.

Yu, X., Dang, X., Li, S., Meng, X., Hou, H., Wang, P., Wang, Q., 2022. Abatement of chlorobenzene by plasma catalysis: Parameters optimization through response surface methodology (RSM), degradation mechanism and PCDD/Fs formation. Chemosphere 298, 134274.

Zhang, Y.-R., Van Laer, K., Neyts, E.C., Bogaerts, A., 2016. Can plasma be formed in catalyst pores? A modeling investigation. Appl. Catal., B 185, 56–67.

Zhang, Y., Wang, H.-y., Zhang, Y.-r., Bogaerts, A., 2017. Formation of microdischarges inside a mesoporous catalyst in dielectric barrier discharge plasmas. Plasma Sources Sci. Technol. 26, 054002.

Zhao, H., Ma, J., Zhang, Q., Liu, Z., Li, R., 2014. Adsorption and diffusion of n-heptane and toluene over mesoporous ZSM-5 zeolites. Ind. Eng. Chem. Res. 53, 13810–13819.

Zhao, Z., Ma, S., Gao, B., Bi, F., Qiao, R., Yang, Y., Wu, M., Zhang, X., 2023. A systematic review of intermediates and their characterization methods in VOCs degradation by different catalytic technologies. Sep. Purif. Technol. 123510.

Zhou, W., Ye, Z., Nikiforov, A., Chen, J., Wang, J., Zhao, L., Zhang, X., 2021. The influence of relative humidity on double dielectric barrier discharge plasma for chlorobenzene removal. J. Clean. Prod. 288, 125502.

Zhu, R., Mao, Y., Jiang, L., Chen, J., 2015. Performance of chlorobenzene removal in a nonthermal plasma catalysis reactor and evaluation of its byproducts. J. Chem. Eng. 279, 463–471.

Zhu, X., Yuan, X., Song, Z., Peng, Y., Li, J., 2024. A dual-balance strategy via phosphate modification on MnO2-CeO2 for NOx and chlorobenzene synergistic catalytic control. Appl. Catal., B 342, 123364.